Seismic Performance of a Precast Hollow Insulated Shear Wall

Zhexian Chen[1], Wenfu He[1], Sen Yang[1(✉)], Cheng Chang[2], and Min Ji[1]

[1] Department of Civil Engineering, School of Mechanics and Engineering Sciences, Shanghai University, Shanghai 200444, China
{chenzhexian,kongxiaosen}@shu.edu.cn

[2] Department of Chemical Engineering, The School of Engineering and Natural Sciences, Heriot-Watt University, Edinburgh EH14 4AS, UK

Abstract. A new precast hollow insulation shear wall (PHISW) is proposed in this paper. To study the seismic behaviors of the new PHISW, two cast-in-place solid shear wall (CSW) specimens, two precast monolithic hollow insulated shear wall (PMW) specimens, and two precast hollow insulated shear wall (PSW) specimens with vertical seams were produced and subjected to low-cyclic reversed loadings. The seismic indices obtained from low-cyclic reversed tests include the failure pattern, hysteretic curves and energy dissipation. The experiment results indicate that flexural failure is the main failure mode of the specimens, but a noticeable difference is detected in the cracking distribution between the three types of shear walls. The bearing capacity of each characteristic point of PMW and PSW is comparable to that of CSW. The ductility coefficient of the newly proposed precast shear wall is slightly lower than that of CSW.

Keywords: Precast hollow insulated shear wall · Low cyclic loading · Bearing capacity · Displacement ductility · Energy dissipation

1 Introduction

In recent years, precast shear walls have been intensively studied and rapidly developed owing to the excellent superiority of a short construction period, less polluting, and good construction quality [1, 2]. However, their relatively large volume and weight limit the wider usage of precast shear walls. Embedding thermal insulation materials (TIMs) in precast shear walls is a reasonable alternative solution, as the TIM can reduce the structural weight and simultaneously enhance the thermal insulation and fire resistance performance [3]. The achieved structure is generally known as the precast hollow insulated shear wall (PHISW). In 1997, Salmon et al. studied the shear resistance performance of a prototype sandwich panel by transverse loading tests [4]. In 1998, Bush et al. proposed a precast sandwich panel with diagonal connectors and explored the flexural performance experimentally and numerically [5]. In 2014, Palermo et al. carried out a shaking table model test on a 3-story building employing precast sandwich shear walls and a corresponding nonlinear numerical simulation on the shear wall components, which proved that structures using the precast sandwich insulation shear wall

could meet the seismic requirements of the current code [6]. Ricci et al. conducted a low cyclic loading test on precast sandwich insulation shear wall specimens, which showed that the precast sandwich insulation shear wall had a larger bearing capacity and better ductility than the cast-in-place shear wall [7].

Current studies of PHISWs are mainly focused on precast sandwich panel walls (PSPWs), which are built up by two outward concrete layers and a middle insulation layer. However, the weakness caused by connectors between the insulation layer and concrete layers and the large requirement of on-site wet work suppresses the applications of PSPWs. For overcoming the above problems, this paper presents a new precast hollow insulated shear wall, which consists of a hollow concrete shear wall and filled-in-hollow polyurethane insulation materials, as shown in Fig. 1. The insulation materials can be directly embedded in the concrete volume at fabrication, which avoids using weak connectors between the thermal insulation material and the concrete.
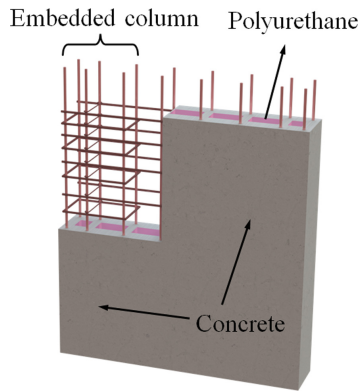

Fig. 1. Precast hollow insulation shear wall.

To analyze the seismic performances of the newly proposed PHISW, 6 shear wall specimens of 3 different configurations were produced and subjected to low-cyclic reversed loading tests. The obtained failure pattern, strength, displacement ductility, and energy dissipation capacity of the specimens were meticulously studied to assess the seismic performance of the new structure.

2 Experimental Investigation

2.1 Test Walls

In this paper, according to the different axial compression ratios, two groups of 6 full-sized specimens were designed, including two cast-in-place solid shear wall (CSW) specimens, two precast monolithic hollow insulated shear wall (PMW) specimens, and two precast hollow insulated shear wall (PSW) specimens with vertical seams, which were designated CSW30, PMW30, PSW30, CSW50, PMW50, and PSW50 (30 and 50 indicate the axial compression ratio by percentage).

The CSW specimens were designed to be 2900 mm high with a cross-section of 1300 mm × 200 mm, as shown in Fig. 2(a). The heights of PMW and PSW were the same as those of CSW, while the cross-section size was 1300 mm × 250 mm, as shown in Fig. 2(b) and (c), because of the insulation fillers. The horizontal reinforcement of the PSW was connected by a straight thread sleeve. The associated parameters of the specimens are presented in Table 1.
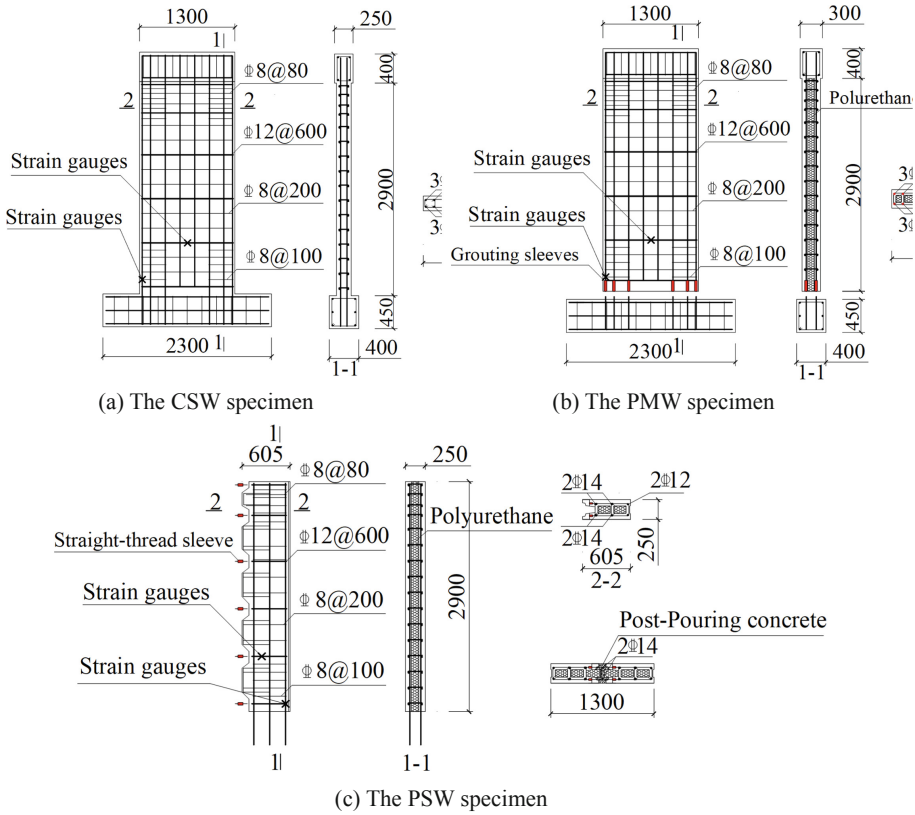
(a) The CSW specimen

(b) The PMW specimen

(c) The PSW specimen

Fig. 2. Details and dimensions of the reinforcements (unit: mm).

2.2 Material Properties

After the test, several concrete core samples with a diameter of 75 mm were picked from the undamaged area of each specimen by drilling. The core drilling method for the compression tests was employed based on the Chinese standard [8]. Table 2 listed the relevant properties of concrete. The strength of reinforcement was measured by a tensile test. The grade of reinforcement used in the shear wall is HRB400, and the diameters are 6 mm, 8 mm, 10 mm, 12 mm, and 14 mm. The achieved yielding and ultimate strengths are summarized in Table 3.

Table 1. Specimen description.

Specimens	Axial compression ratio	Construction forms	Section size (mm)
CSW30	0.3	Cast-in-place solid wall	200 × 1300
PMW30	0.3	Precast monolithic hollow insulated wall	250 × 1300
PSW30	0.3	Precast hollow insulated wall with vertical seams	250 × 1300
CSW50	0.5	Cast-in-place solid wall	200 × 1300
PMW50	0.5	Precast monolithic hollow insulated wall	250 × 1300
PSW50	0.5	Precast hollow insulated wall with vertical seams	250 × 1300

Table 2. Properties of concrete.

Category	Class	f_{cu} (MPa)
CSW30	C35	32.6
PMW30	C50	52.7
PSW30	C50	52.8
CSW50	C35	51.7
PMW50	C50	52.6
PSW50	C50	47.3

Table 3. Properties of steel reinforcements.

Category	f_y (MPa)	f_u (MPa)
6	–	612.5
8	–	646.1
10	–	633.7
12	453	616.3
14	436	641.5

Note: After cold treatment, the yield strength of steel bars with diameters of 6, 8, and 10 was not measured.

2.3 Experimental Setup and Measuring System

The schematic of the loading device is shown in Fig. 3. Considering that the PMW and PSW were hollow, their bearing capacity was uncertain, so the axial pressure of the pre-cast specimen was determined according to the CSW. The corresponding vertical loads under axial compression ratios of 0.3 and 0.5 are 1340 kN and 2240 kN, respectively.

As shown in Fig. 3, the applied loadings generated by the hydraulic actuator were measured by transducers built inside. The displacement of the top of the wall was gauged using LVDT-1. The transducer LVDT-2 for monitoring the displacement of the bottom beam ensured that the bottom beam had no slippage displacement. In addition, high-precision sensors were installed to the longitudinal reinforcements and stirrups at the reference points, as represented in Fig. 2, monitoring the rebar strain state. A hybrid loading protocol alternately controlled by force and displacement was employed in horizontal loading, as illustrated in Fig. 4.
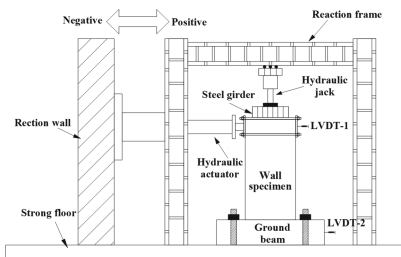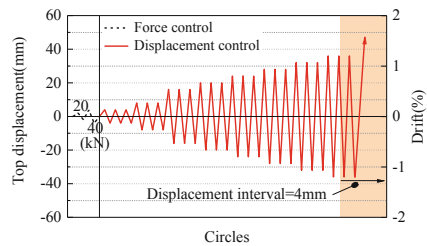

Fig. 3. Test setup.

Fig. 4. Loading protocol.

3   Experimental Results

3.1 Cracks and Failure Patterns

The six specimens exhibited similar breakage patterns dominated by flexural failure, including concrete spalling in the corners, and the appearance of bend and shear cracks at both sides of the wall. Typically, the seismic capacity of the reinforced concrete shear wall can be evaluated with crack distribution [9, 10]. Figure 5 reveals the crack distribution of the 6 specimens.

However, the evolution of the cracks differed markedly. The number of cracks of specimens under an axial compression ratio of 0.5 was significantly less than those of 0.3. The cracks of the CSW and PMW were evenly distributed with abundant development compared with the PSW specimens. This could be attributed to the gap growth of the vertical assembling seam in the PSW, which led to insufficient crack propagation. Because of the existence of a vertical assembling seam, PSW specimens had fewer shear cracks, which can make full use of the strength of the material [11].
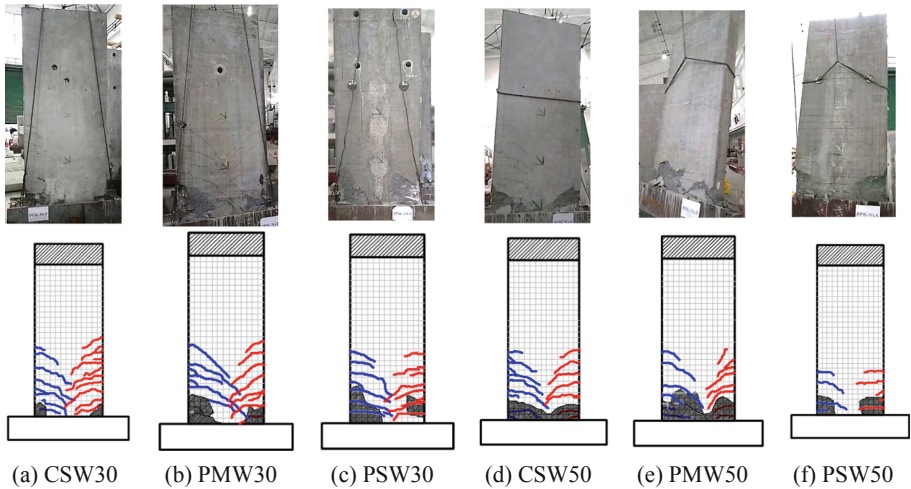
(a) CSW30	(b) PMW30	(c) PSW30	(d) CSW50	(e) PMW50	(f) PSW50

Fig. 5. Crack patterns under cyclic loading.

3.2 Strain Distributions of the Reinforcement Rebars

The strain distributions of the vertical reinforcement bars measured by the arranged gauges are plotted in Fig. 6. Before the specimen cracked, the strain of the longitudinal reinforcements in the most lateral of the wall appeared linearly. In the plastic phase, with the neutral axis of the specimen moving to the compression side, the strain of the vertical tension reinforcement was far larger than that of the compressed reinforcement. The longitudinal bars of the PMW specimens yielded earlier than those of the CSW and PSW.

Figure 7 demonstrates the strain evolution ruler of the middle stirrup of the wall at a height of 650 mm from the ground beam. The strain developed slowly before the horizontal displacement reached 20 mm. However, due to the extension of flexural-shear cracks, when the horizontal displacement was larger than 20 mm, the stirrup strain increased significantly, and the ultimate strain of the PMW specimens was larger than that of the other two types of specimens.

3.3 Hysteresis Behavior and Envelope Curves

The property of hysteretic loops of the specimens is illustrated in Fig. 8. At the beginning of loading, all specimens worked elastically, and the hysteresis loop area, i.e., the dissipated energy, was rather small. With increasing loading displacement, the specimens gradually participated in the elastic-plastic phase, and the area of the hysteresis curve increased gradually. The stiffness of the specimen decreased obviously after reaching the peak load, and the pinching phenomenon began to appear in the hysteresis curves. In the end, the hysteretic area of the PSW specimens was smaller than that of the other two types of specimens according to the slight slip of the straight thread sleeves under high-stress repeated loading.
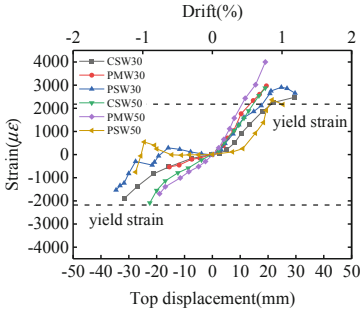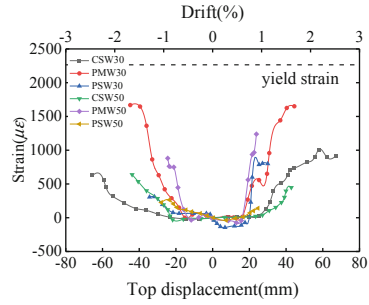
Fig. 6. The strain of vertical reinforcement.

Fig. 7. The strain of stirrup.

(a) CSW30

(b) PMW30
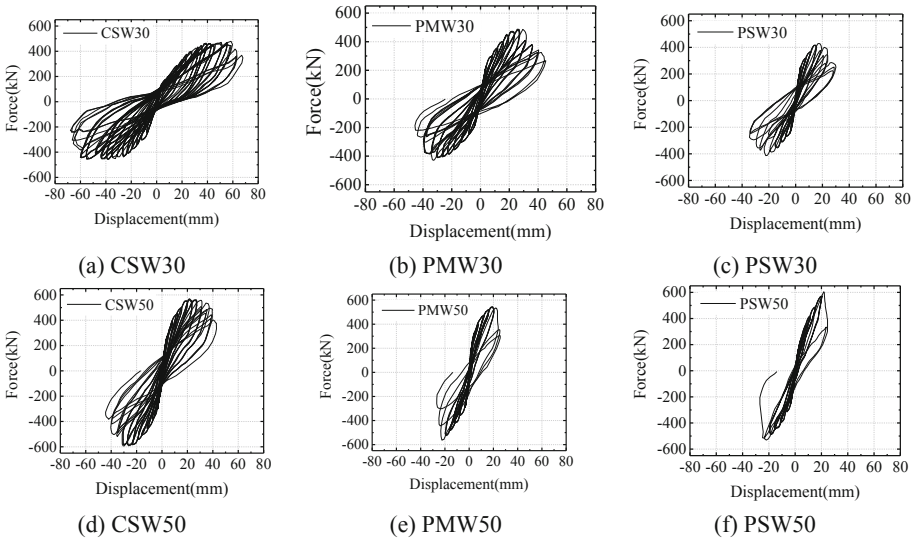
(c) PSW30

(d) CSW50

(e) PMW50

(f) PSW50

Fig. 8. Hysteresis loops.

Table 4 listed the cracking load F_{cr}, yielding load F_y and peak load F_P of the specimens. The mean values of F_y of PMW30 and PSW30 were approximately 3.6% and 13.1% lower than those of CSW30, respectively. Under the same axial pressure, the average F_P values of PMW30 and PSW30 were 2.1% and 9.8% lower than those of CSW30, respectively. The bearing capacity at feature points of wall specimens with an axial load ratio of 0.5 is greater than those with small axial pressure. Significantly, the F_{cr} values of PSW30 and PSW50 were 7.9% and 8.4% greater than those of CSW30 and CSW50, respectively. Because of the existence of the vertical assembling seam, PSW specimens can convert the overall shear failure of the ordinary shear wall into the bending failure of each wall limb element and can capitalize the strength of the material [11].

Table 4. The bearing capacity of the characteristic points (unit: kN).

Specimens	F_{cr}			F_y			F_P		
	Pos	Neg	Ave	Pos	Neg	Ave	Pos	Neg	Ave
CSW30	287.15	281.08	284.12	410.22	380.31	395.26	477.32	460.98	469.15
PMW30	297.45	238.38	267.92	398.10	363.95	381.03	485.98	432.33	459.16
PSW30	329.81	283.58	306.70	353.40	333.25	343.32	428.84	417.64	423.24
CSW50	387.80	412.10	399.95	468.59	486.17	477.38	565.91	593.53	579.72
PMW50	312.51	416.35	364.43	448.59	448.47	448.53	543.20	556.86	550.03
PSW50	442.91	424.50	433.71	508.35	427.35	467.85	602.80	525.60	564.20

Table 5. Displacement at feature point (mm) and ductility coefficient.

Specimens	Δ_{cr}		Δ_y		Δ_μ		μ		Ave
	Pos	Neg	Pos	Neg	Pos	Neg	Pos	Neg	
CSW30	16.04	12.10	29.54	19.64	62.58	59.47	2.12	3.03	2.48
PMW30	8.09	8.66	15.05	18.97	31.96	36.82	2.12	1.94	2.03
PSW30	8.70	8.09	10.22	12.64	21.26	28.03	2.08	2.22	2.15
CSW50	8.00	8.12	13.09	13.39	37.99	37.99	2.90	2.84	2.87
PMW50	4.34	12.55	10.42	13.50	23.45	23.93	2.25	1.77	2.01
PSW50	12.14	12.45	16.49	13.79	23.08	24.81	1.40	1.80	1.60

3.4 Ductility

As the axial load ratio increased, the ductility of PMW and PSW was reduced. The ductility coefficients of PMW30 and PSW30 were 18.1% and 13.4% lower than those of CSW30, respectively. However, the ultimate drifts were 1.21% and 0.85%, respectively, which were larger than the criterion of 1/120 (0.83%) specified by Chinese codes [12]. The ductility coefficients of PMW50 and PSW50 with a designed axial compression ratio of 0.50 were 29.9% and 44.3% lower than those of CSW50, and their ultimate drifts were 0.817% and 0.828%, respectively, which were slightly smaller than the limit value of 1/120 (0.83%). Therefore, the four precast hollow insulated shear wall specimens exhibited good ductility. It's worth noting that the ductility of PSW was better under an axial compression ratio of 0.3, because larger axial pressure would weaken the structural integrity (Table 5).

3.5 Energy Dissipation

Energy-absorbing ability can also be used to evaluate seismic performance [13]. The cumulative hysteretic energy E and equivalent viscous damping coefficient h_e are normally used in seismic analysis of structures [14]. Figure 9 shows the cumulative energy

dissipation of specimens E. And the equivalent viscous damping coefficient h_e is exhibited in Fig. 10. From the diagram, the trends of the E and h_e of the three types of 6 specimens were almost the same. The equivalent viscous damping coefficient h_e of the PMW and CSW increased faster along with enhanced axial pressure, but that of the PSW did not change significantly. This means that due to the existence of a vertical seam, PSW was less vulnerable to the influence of the axial force.
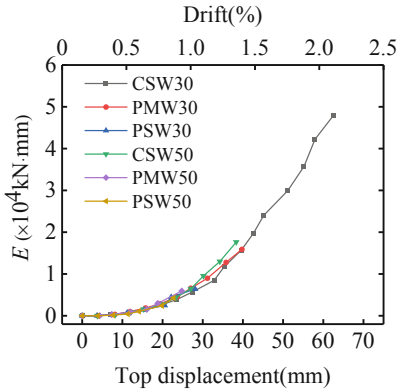

Fig. 9. Cumulative energy dissipation.
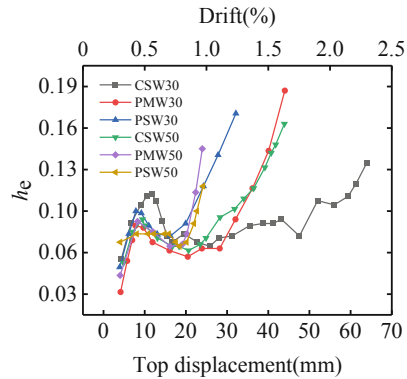
Fig. 10. Equivalent viscous damping coefficient.

4   Conclusions

In this paper, a new precast shear wall filled with polyurethane materials for thermal insulation is put forward and investigated. A low cyclic loading test was carried out about six full-scale specimens, which include two cast-in-place solid shear wall specimens, two precast monolithic hollow insulated shear wall specimens, and two precast hollow insulated shear wall specimens with vertical seams. Based on the test results, some meaningful conclusions can be achieved:

(1) Bending failure was the primary destructive mode of cast-in-place and precast walls, although the crack distributions were different. The cracks of the cast-in-place wall are denser than those of the precast wall. In addition, the cracks of the PSW continuously ran through the vertical seams of the wallboard, which manifested that the PSW had a good cooperative performance.

(2) The peak bearing capacity of the precast shear wall newly brought forward was close to that of the cast-in-place wall. And the hysteretic area of the PMW was larger than that of the PSW.

(3) The ductility of the two kinds of precast walls was slightly worse than that of the cast-in-place walls under the two axial compression ratios. However, the ductility coefficient of the precast wall came close to the value of Chinese specification, which indicated good ductility performance of the precast wall.

References

1. Wang, Z., Pan, W., Zhang, Z.Q.: High-rise modular buildings with innovative precast concrete shear walls as a lateral force resisting system. Structures **26**, 39–53 (2020)
2. Smith, B.J., Kurama, Y.C., McGinnis, M.J.: Behavior of precast concrete shear walls for seismic regions: comparison of hybrid and emulative specimens. J. Struct. Eng. **139**, 1917–1927 (2013)
3. Michele, P., Tomaso, T.: Experimentally-validated modeling of thin RC sandwich walls subjected to seismic loads. Eng. Struct. **119**, 95–109 (2016)
4. Salmon, D.C., Eiena, A., Tadros, M.K., Culp, T.D.: Full scale testing of precast concrete sandwich panels. ACI Struct. J. **94**, 354–362 (1997)
5. Bush, T.D., Wu, Z.: Flexural analysis of prestressed concrete sandwich panels with truss connectors. PCI J. **43**, 76–86 (1998)
6. Palermo, M., Ricci, I., Silvestri, S., et al.: Preliminary interpretation of shaking-table response of a full-scale 3-storey building composed of thin reinforced concrete sandwich walls. Eng. Struct. **76**, 75–89 (2014)
7. Ricci, I., Palermo, M., Gasparini, G., Silvestri, S., Trombetti, T.: Results of pseudo-static tests with cyclic horizontal load on cast in situ sandwich squat concrete walls. Eng. Struct. **54**, 131–149 (2013)
8. JGJ/T384-2016: Technical Specification for Testing Concrete Strength with Drilled Core Method. China Architecture Industry Press (2016)
9. Ebrahimkhanlou, A., Farhidzadeh, A., Salamone, S.: Multifractal analysis of crack patterns in reinforced concrete shear walls. Struct. Health Monitor.-An Int. J. **15**, 81–92 (2016)
10. Zhi, Q., Guo, Z.X., Xiao, Q.D., et al.: Quasi-static test and strut-and-tie modeling of precast concrete shear walls with grouted lap-spliced connections. Constr. Build. Mater. **150**, 190–203 (2017)
11. Cui, Z.: An experimental research on seismic behavior of reinforced concrete hollow shear wall with vertical seams. Xi'an University of Architecture and Technology (2004)
12. GB 50011-2010: Code for seismic design of buildings. China Architecture Industry Press (2010)
13. Rao, G.A., Poluraju, P.: Cyclic behaviour of precast reinforced concrete sandwich slender walls. Structures **28**, 80–92 (2020)
14. JGJ/T101-2015: Specification for Seismic Test of Buildings. China Architecture Industry Press (2015)